A CHROMOSPHERIC RESPONSE TO PULSE BEAM HEATING

PETR HEINZEL

Astronomical Institute, 251 65 Ondřejov, Czechoslovakia

(Received 5 February, 1991; in revised form 16 April, 1991)

Abstract. Starting from the new flare models of Karlický (1990) and Karlický and Hénoux (1991), we present here the first time-dependent numerical simulations of hydrogen plasma excitation and ionization on time scales of less than one second. These time scales are consistent with the spiky behaviour of the kinetic temperature produced by non-thermal collisional processes. Such temperature spikes represent a chromospheric response to a series of short-duration electron beam pulses which are supposed to heat the flare atmosphere. Self-consistent numerical solution of a simplified, time-dependent, non-LTE problem for a three-level hydrogen atom model with continuum allows us to predict theoretically a qualitative behaviour of the Hα line intensity variations on very short time intervals. Our Hα temporal profiles, evaluated at the line center and for $\Delta\lambda = 1$ Å, can be qualitatively compared with some recent flare observations obtained with high temporal resolution.

1. Introduction

The impulsive phase of the solar flares is manifested by a typically enhanced chromospheric radiation in the Hα line, temporally correlated with the hard X-ray (HXR) emission and microwaves. Recently, some authors have indicated that the corresponding time correlations seem to occur on very short time scales on the order of one second, which is at the resolution limit of the available Hα instruments (Kurokawa, 1986; Kitahara and Kurokawa, 1990; Graeter, 1990; see also references cited in these papers). However, higher temporal resolution, reaching 0.1 s, is now being achieved by a High-Speed Hα Camera operating within MAX'91 campaigns (Kiplinger *et al.*, 1988). For example, Graeter (1990) presents the observed temporal variations of Hα line-center and $\pm$ 1.75 Å wing intensities for September 8, 1988 flare, with the resolution of 2.3 s. Like the corresponding HXRBS data, Hα exhibits a series of short-duration spikes. At this temporal resolution, a degree of correlation between individual Hα and HXR spikes seems to be rather good, although one can identify some 'inverse' spikes in Hα (decreasing intensity) at the time of rapid HXR increase.

All these features seem to represent a response of the denser chromosphere to accelerated particle beams (electrons and/or protons), which are commonly supposed to heat the lower atmospheric layers (for reviews see, e.g., Kundu, Woodgate, and Schmahl, 1989). However, the existing theoretical models of a beam-heated chromosphere are confined only to a stationary or quasi-stationary heating lasting several seconds or tens of seconds (Fischer, Canfield, and McClymont, 1985a–c; hereafter FCM; Mariska, Emslie, and Li, 1989). In these studies, the beam of energetic electrons is considered schematically as an extra heating term in the corresponding energy balance equation, neglecting both the finite travel time of electrons in the flare loops and the details of their interaction with particles of the chromospheric plasma. Only recently,

Solar Physics **135:** 65–88, 1991.

Karlický (1990) and Karlický and Hénoux (1991) have numerically simulated electron beams of very short duration (beam pulses lasting less than one second) and evaluated the chromospheric response to such a pulse (Karlický, 1990) and to a series of identical pulses (Heinzel and Karlický, 1991). It is quite possible that a series of several beam pulses produces the impulsive phase of the chromospheric flare rather than a continuous, more or less stationary beam, as was previously expected (note that in some previous studies the authors considered beams lasting tens of seconds (Brown, 1973) or purely stationary situations (e.g., Ricchiazzi and Canfield, 1983).

In order to simulate, at least qualitatively, the temporal behaviour of the Hα emission in the presence of a series of short-duration beam pulses, we solve here a simplified time-dependent non-LTE problem for a three-level hydrogen atom with continuum. For one pulse lasting 5 s, a similar problem was recently treated by Canfield and Gayley (1987), who used the radiation-hydrodynamical simulations of FCM as the input model atmosphere. We discuss their computations in Section 6 and compare them with our simulations. However, our multi-spike non-LTE simulations are based on new models of Karlický (1990), which we briefly describe in the next Section 2. In Sections 3 and 4 we summarize all computational aspects of our approach and Sections 5 and 6 contain several numerical results which we discuss in detail. The most important goal of the present paper is to study the behaviour of short-duration Hα spikes arising from the beam heated flare plasma with rather long relaxation times, so that a consistent time-dependent solution of hydrogen rate equations is required at least for three-level plus continuum model atom.

2. Pulse Beam Heating Models

As an input for our non-LTE modeling, we use the results of hydrodynamical simulations of Karlický (1990) and Heinzel and Karlický (1991). Starting with the quiet-Sun atmosphere models of Vernazza, Avrett, and Loeser (1981) (VAL3C-model), Karlický (1990) has used a special particle code to generate accelerated electron beams with a given energy distribution which enter the chromosphere at the time $t = 0$. Then the quiet atmosphere is heated due to the electron-beam energy dissipation and further temporal development of the flaring hydrogen plasma is governed by a standard set of hydrodynamical and energy-balance equations. The energy equation contains the heating term computed – in contrast to previous work – from particle simulations (for details see Karlický, 1990). It is also shown that the radiation cooling dominates other cooling mechanisms (e.g., conduction). However, the proper evaluation of the radiative losses is closely linked with the temporal behaviour of the hydrogen excitation and ionization, so that the energy-balance equation must be solved simultaneously with time-dependent hydrogen rate equations. In fact, this was done for a two-level plus continuum hydrogen atom by FCM. From this viewpoint, Karlický's simulations are less consistent since he uses Brown's (1973) modified Saha ionization formula, which can be justified only at higher plasma densities. But on the other hand, new simulations of Karlický (1990) are so complex that this approximation was necessary at first step (a modification of the

code towards more consistent solutions is now in progress). For these reasons, we do not use $n_e(t)$ (electron density) computed by Karlický as the input for our set of rate equations (as was done for example by Canfield and Gayley (1987) using FCM's two-level atom simulations), but rather we start from his temporal profiles $T(t)$ and solve consistently the time-dependent problem for a three-level atom with continuum. Of course, these temperature profiles will be quantitatively somewhat different if the ionization and excitation of hydrogen (and other important species) is computed consistently, but we use them only as a guide in order to have some more or less realistic input for our simulations. Therefore, for typical chromospheric layers we specify $T(t)$ in an analytical form as one temperature pulse or a series of such identical pulses, starting from $T_0 = 6500$ K and reaching the maximum value $T_m = 10^4$ K. The heating and cooling times are also consistent with the results of Karlický's (1990) simulations and are specified in Section 5.

Although the beam energy flux is comparable to that used by other authors (e.g., FCM), short-duration heating lasting around 0.1 s is barely able to deposit a sufficient amount of energy required to move the plasma. Therefore, for our numerical simulations we use a static model atmosphere with constant total hydrogen number density. The effects of plasma evaporation and stronger velocity fields can be produced by modifying the initial eneregy flux of the beam or by using a higher frequency of very short pulses. However, at high-energy fluxes the electron beams generate a return current which is difficult to account for.

In our simplified non-LTE analysis, we replace net radiative brackets in the rate equations by the respective escape probability functions for Hα and Lyman continuum (Lc) transitions, while both Lyman lines are put into detailed radiative balance in the atmospheric region where the Hα line is formed. Subordinate continua are optically thin with their radiative rates fixed by the photospheric radiation temperatures. Time-dependent hydrogen rate equations are then solved only for two slabs which represent the Hα line core and line-wing formation regions. All details of this approach are described in the following Sections 4 and 5. Typical hydrogen densities n_{H}, temperature profiles $T(t)$, and the rates of the electron-beam energy deposit $\mathrm{d}F/\mathrm{d}z$ are consistent with Karlický's (1990) models, although we also add some other values to demonstrate a broader range of possible situations.

3. Time-Dependent Rate Equations

We consider a pure hydrogen plasma consisting of three-level neutral atoms, protons, and electrons. Denoting n_k and n_e as the proton (k is the continuum state) and electron density, respectively, we can write the charge conservation condition

$$n_k = n_e \,. \tag{3.1}$$

Time-dependent rate equations used in our simulations have the general form (Mihalas, 1978)

$$\partial n_i/\partial t = \sum_{j \neq i} (n_j P_{ji} - n_i P_{ij}) \quad (i = 1\text{–}3)\,, \tag{3.2}$$

where n_i represents the number density of hydrogen atoms in a particular bound state i. P_{ij} and P_{ji} are the total transition rates (both radiative R_{ij} and collisional C_{ij}) from the level i and into it, respectively. In a *steady state* all level populations are time-independent, i.e., $\partial n_i/\partial t = 0$ in Equations (3.2). As already mentioned in the previous section, we consider here a static atmosphere. In order to close the set of Equations (3.2), we use the hydrogen total number conservation condition

$$\sum_{i=1}^{3} n_i + n_k = n_{\mathrm{H}} , \tag{3.3}$$

where the total hydrogen number density n_{H} is kept constant in the present static case.

Although non-LTE rate Equations (3.2) are purely local ones, they contain the radiative terms R_{ij} which, in turn, depend explicitely on the radiation field in a given transition $i \rightarrow j$, and this radiation field has a non-local character. A solution of (3.2), which is nonlinearly coupled to the radiative transfer equations and other constraint equations, represents a difficult numerical task even in the steady-state case (Mihalas, 1978; Heinzel, Gouttebroze, and Vial, 1987). For a two-level hydrogen atom with continuum, the time-dependent non-LTE problem, coupled to the other hydrodynamic and energy-balance equations, was solved by FCM, using the probabilistic transfer equation. These authors obtained several very important results for a steady-state heating situation.

In order to study the temporal behaviour of hydrogen excitation and ionization, we use here the following approach to radiative transfer. Within the chromospheric layers we assume the detailed radiative balance $n_1 R_{1j} = n_j R_{j1}$ in both Lyman lines, since these transitions are supposed to be optically thick in the flare layers where Hα is formed. On the other hand, for the Hα line and for Lyman continuum we can assume neither optical thinness, nor a detailed radiative balance (except in the deep chromospheric layers). In order to avoid complicated and time-consuming transfer solutions, we work here in terms of the escape probability for these transitions. Finally, both subordinate continua are optically thin. Using all these assumptions, we can write the time-dependent rate equations for our three-level atom in the form

$$\begin{aligned} \partial n_1/\partial t = {} & n_2 C_{21} + n_3 C_{31} + n_k C_{k1} + n_k R_{k1} \rho_{k1} - n_1 (C_{12} + C_{13} + C_{1k}) - \\ & - n_1 (C_{12}^{nt} + C_{13}^{nt} + C_{1k}^{nt}) \equiv f_1 , \end{aligned} \tag{3.4a}$$

$$\begin{aligned} \partial n_2/\partial t = {} & n_1 C_{12} + n_3 C_{32} + n_k C_{k2} + n_1 C_{12}^{nt} + n_k R_{k2} + n_3 A_{32} \rho_{32} - \\ & - n_2 (C_{21} + C_{23} + C_{2k} + R_{2k}) \equiv f_2 , \end{aligned} \tag{3.4b}$$

$$\begin{aligned} \partial n_3/\partial t = {} & n_1 C_{13} + n_2 C_{23} + n_k C_{k3} + n_1 C_{13}^{nt} + n_k R_{k3} - n_3 A_{32} \rho_{32} - \\ & - n_3 (C_{31} + C_{32} + C_{3k} + R_{3k}) \equiv f_3 , \end{aligned} \tag{3.4c}$$

where we have replaced P_{ij} by $R_{ij} + C_{ij}$ and included the non-thermal collisional rates C_{ij}^{nt} (see below). In a steady state we get $f_i = 0$. Radiative rates for the Hα transition, appearing in Equations (3.4b) and (3.4c), are expressed through the net radiative bracket

ρ_{32}, i.e.,

$$n_3 A_{32} \rho_{32} = n_3 R_{32} - n_2 R_{23} = n_3 A_{32} + n_3 B_{32} \bar{J}_{23} - n_2 B_{23} \bar{J}_{23} , \tag{3.5}$$

where A_{32}, B_{32}, and B_{23} are the Einstein coefficients and $\bar{J}_{23} = \int \varphi(\nu) J(\nu) \, d\nu$ is the mean integrated intensity of the Hα radiation field. The mean intensity $J(\nu)$, which is here weighted by the absorption profile $\varphi(\nu)$, must generally be determined from the solution of the transfer equation. However, as follows from the analysis of Canfield, Gunkler, and Ricchiazzi (1984), under flare conditions the Hα line source function is controlled rather by interlocking transitions than by the line radiation field in Hα itself and thus the accuracy of $\bar{J}_{23}$ is not so critical in our simulations. An approximate way of computing ρ_{32} is to apply the so-called first-order escape probability technique, in which ρ_{32} can be replaced by the escape-probability function P_e (see, e.g., Rybicki, 1984):

$$\rho_{32} \cong P_e = K_2(\tau)/2 . \tag{3.6}$$

The kernel function $K_2(\tau)$, depending on the line optical depth τ, can be evaluated using the expansions of Hummer (1982) for both gaussian and Voigt line profiles. Since $K_2(\tau) \to 0$ for $\tau \to \infty$, we arrive at the condition $\rho_{32} \cong P_e \to 0$ at great depths, i.e., the escape probability of an Hα photon during a single flight goes to zero and from (3.5) we get the condition of detailed radiative balance even for Hα. On the other hand, at the atmospheric levels where $\tau(\mathrm{H}\alpha) \to 0$ (in the middle chromosphere), $K_2(\tau) \to 1$ and thus $\rho_{32} \cong P_e \to \frac{1}{2}$. This can easily be understood since half of all photons escapes from the atmosphere and the second half of them goes down and are ultimately absorbed. In the present exploratory work we shall concentrate ourselves only on these two limiting cases which correspond to the situation in a deep layer and at the surface where Hα becomes optically thin (more detailed transfer computations will be reported in another paper). For this reason we use an approximate formula valid for a Voigt profile (Ivanov, 1973; Dumont and Collin-Souffrin, 1985):

$$P_e = \begin{cases} \frac{1}{2}[1 + 2\tau\sqrt{\pi \ln(\tau + 1)}]^{-1}, & \tau < a^{-1}, \\ \frac{1}{3}[a/\tau\sqrt{\pi}]^{1/2}, & \tau \geq a^{-1}, \end{cases} \tag{3.7}$$

where a is the common damping parameter appearing in the Voigt function and τ represents the line-center optical depth. However, as demonstrated by Dumont and Collin-Souffrin (1985), the Hα line core as formed in the quiet solar chromosphere is not well described when assuming $\rho_{32} \cong P_e$ at $\tau \to 0$. In fact, $\rho_{32} < P_e$ in the region $\tau < 2$–10 and, therefore, Dumont and Collin-Souffrin (1985) have proposed an empirical modification to the above formula in order to fit the quiet-Sun Hα line core. Hα line source function is improved if one replaces τ by τ_c for $\tau < \tau_c$, where $\tau_c = 3$. In our 3-level model atom simulations, we arrived at even larger 'critical' optical depth $\tau_c \cong 5$. Since $\tau_c = 5$ is typically less than a^{-1} for most conditions considered here, we set $\rho_{32} = P_e = 0.02$ at the surface of Hα emitting layer (which is really much lower than $\frac{1}{2}$) and $\rho_{32} = 0$ at large depths.

Concerning the Lyman continuum (Lc), Brown (1973) has assumed that Lc is in

detailed radiative balance under flare conditions. Dumont and Collin-Souffrin (1986) also put Lc into detailed radiative balance in the case of the quiet solar chromosphere. In fact, the situation is as follows: we can see from VAL3C model of Vernazza, Avrett, and Loeser (1981) (see their Figure 30) that $\tau(\mathrm{Lc}) \cong 10$–$100$ in the region where Hα core is formed. On the other hand, as we shall see in Section 5, during the flare heating, the hydrogen ground level is depopulated and thus $\tau(\mathrm{Lc})$ is lowered, while $\tau(\mathrm{H}\alpha)$ simultaneously increases – this is also evident from semi-empirical flare models of Avrett (1988). In fact, Hα is still optically thick in the flare regions where Lyman continuum becomes thin. Therefore, we can not assume detailed radiative balance in Lc at the surface where the Hα core is formed and we use an approach of Canfield and Puetter (1981) (see also Canfield and Ricchiazzi, 1980). These authors have proposed a simple approximation especially valid for Lc, namely that $\rho_{k1} \cong P_e^c$, where P_e^c for the continuum transition can be evaluated according to formulae (23) or (24) in Canfield and Ricchiazzi (1980). However, the dependence of P_e^c on the Lc head opacity, as shown in Figure 1 of these authors, indicates that $P_e^c(\tau) \cong \frac{1}{2}$ for $\tau(\mathrm{Lc}) < 0.1$. Since the Hα line core is formed approximately in this region, we set $\rho_{k1} = P_e^c = \frac{1}{2}$. For H$\alpha$ wings, a good approximation is to set $\rho_{k1} = 0$. Of course, both ρ_{32} as well as ρ_{k1} are generally time-dependent, but the above approximations seem to be adequate for our qualitative analysis. Now, we briefly describe the methods of computing the remaining rates appearing in Equations (3.4). Radiative rates for ionization and recombination in optically-thin subordinate continua (Balmer and Paschen) are held fixed and are determined in a usual way by using the radiative temperature T_r of the photospheric radiation field and the electron temperature T_e. For the photoionization rates we then write (Mihalas, 1978)

$$n_i R_{ik} = n_i 4\pi \int_{\nu_0}^{\infty} \alpha_{ik}(\nu) J(\nu)/h\nu \, \mathrm{d}\nu \cong n_i 4\pi \int_{\nu_0}^{\infty} \alpha_{ik}(\nu) W B_\nu(T_r)/h\nu \, \mathrm{d}\nu , \tag{3.8}$$

where we have approximated the incident continuum intensity $J(\nu)$ by the diluted photospheric radiation field $WB_\nu(T_r)$ with the dilution factor W. According to Auer, Heasley, and Milkey (1972), we rewrite the integral in (3.8) to read

$$R_{ik} = (8\pi/c^2) W \alpha_{ik}(\nu_0) \nu_0^3 \sum_{n=1}^{\mathcal{N}} E_1(nh\nu_0/kT_r) , \tag{3.8a}$$

where $\alpha(\nu_0)$ is the head opacity of the ith continuum, ν_0 is the head frequency, and E_1 denotes the first exponential integral. For the radiative recombinations, including the Lyman continuum, we get (see also Mihalas, 1978)

$$n_k R_{ki} = n_k (n_i/n_k)^* 4\pi \int_{\nu_0}^{\infty} (2h\nu^3/c^2) \, e^{-h\nu/kT_e} \, \alpha_{ik}(\nu)/h\nu \, \mathrm{d}\nu \cong$$

$$\cong n_k (n_i/n_k)^* 4\pi \int_{\nu_0}^{\infty} \alpha_{ik}(\nu) B_\nu(T_e)/h\nu \, \mathrm{d}\nu , \tag{3.9}$$

$$R_{ki} = (n_i/n_k)^* (8\pi/c^2) \alpha_{ik}(\nu_0) \nu_0^3 \sum_{n=1}^{\mathcal{N}} E_1(h\nu_0/kT_e) .$$

In Equation (3.9) we have neglected the stimulated recombination term. The ratio of LTE-level populations $(n_i/n_j)^*$ (the asterisk denotes LTE) is expressed through the corresponding Boltzmann factors $\Phi_i(T_e)$ (Mihalas, 1978) as

$$(n_i/n_k)^* = n_e \Phi_i(T_e)\,, \tag{3.10}$$

$$\Phi_i(T_e) = 2.07078 \times 10^{-16} g_i T_e^{-3/2} e^{h\nu_i/kT_e}\,, \tag{3.11}$$

where $n_e = n_k$, g_i is the statistical weight of the ith level (for hydrogenic levels $g_i = 2i^2$) and ν is the ionization frequency from the level i. The radiation temperatures T_r have been taken from Heinzel, Gouttebroze, and Vial (1987). These temperatures do not include the dilution factor which appears explicitely in the above equations. We use $T_r = 5480$ K and $T_r = 5900$ K for Balmer and Paschen continuum, respectively. At the middle chromosphere we set approximately $W = \frac{1}{2}$.

Collisional rates for hydrogen have the general form

$$\begin{aligned} n_i C_{ij} &= n_i n_e \Omega_{ij}(T_e)\,, \quad i < j,\ j = 2 - k\,, \\ n_j C_{ji} &= n_j (n_i/n_j)^* C_{ij} = n_j (g_i/g_j)\, e^{-h\nu_i/kT_e} C_{ij}\,, \quad i < j,\ j \neq k\,, \\ n_k C_{ki} &= n_k n_e \Phi_i(T_e) C_{ik} = n_k n_e^2 \Phi_i(T_e) \Omega_{ik}(T_e)\,, \quad i < k\,; \end{aligned} \tag{3.12}$$

C_{ki} is the rate of three-body collisional recombinations. Temperature-dependent function $\Omega_{ij}(T_e)$ has been computed with the numerical routine taken from Auer, Heasley, and Milkey (1972).

Non-thermal processes (hydrogen ionization and excitation) have also been taken into account during the beam heating. According to Aboudarham and Hénoux (1986), we consider here the non-thermal collisional excitation rates C_{12}^{nt}, C_{13}^{nt}, and the ionization rate C_{1k}^{nt} which arise due to collisional interactions with an electron beam. The inverse non-thermal processes can be neglected (Feautrier and Sahal-Bréchot, 1991). Excitation rates are related to the ionization one as follows (see Aboudarham and Hénoux, 1986):

$$C_{12}^{nt} = 1.35 C_{1k}^{nt} \quad \text{and} \quad C_{13} = 0.20 C_{1k}^{nt}\,. \tag{3.13}$$

Therefore, we need to evaluate only the ionization rate which can be expressed as (Ricchiazzi and Canfield, 1983)

$$C_{1k}^{nt} = (3.78 \times 10^9 \Lambda'/n_{\mathrm{H}}\gamma)\, \mathrm{d}F/\mathrm{d}z\,, \tag{3.14}$$

where $\mathrm{d}F/\mathrm{d}z$ represents the total energy deposit rate of the beam electrons, n_{H} is the hydrogen particle density (protons and neutrals), $\gamma = \Lambda x + \Lambda'(1 - x)$ with the ionized fraction $x = n_e/n_{\mathrm{H}}$. Λ and Λ' are, respectively, the Coulomb logarithms for collisions with ambient electrons and neutral hydrogen atoms. According to Emslie (1978), we can write

$$\Lambda = \ln(v^3/\sqrt{n_e}) - 29.146\,, \qquad \Lambda' = \ln(v^2) - 37.811\,; \tag{3.15}$$

v is the initial beam velocity, which we take here to be $v = 10^{10}$ cm s^{-1} for all our models (Karlický, 1990). Note that the logarithmic dependence on v is rather weak in both these expressions. Energy deposit $\mathrm{d}F/\mathrm{d}z$ is not evaluated here and is taken as a free parameter,

just to demonstrate the importance of non-thermal processes. In the numerical simulations, we allow C_{1j}^{nt} ($j = 2, 3, k$) to be non-zero during the heating process when the beam-pulse is switched-on. In fact, we use an exponential increase of non-thermal collisional rates, multiplying them by a factor $[1 - \exp(-5(t - t_0)/\Delta t_h)]$, where t_0 is the time when the pulse is switched-on and Δt_h represents the heating time (0.1 s in most of our models).

4. Numerical Solution

In this section we shall discuss the numerical solution of Equations (3.3) and (3.4) which represent a set of nonlinear first-order differential equations. Their non-linearity is evident from Equations (3.9), (3.10), and (3.11), where the recombination rates, multiplied by the density of kth state particles $n_k = n_e$ lead to nonlinear terms proportional to n_e^2 for radiative recombination and to n_e^3 for collisional three-body recombination. Since we are primarily interested in the temporal behaviour of hydrogen ionization, i.e., in the temporal variations of the electron density n_e, we must solve the set (3.3) together with (3.4) consistently with respect to these nonlinear terms.

As a basic time difference scheme for solving first-order differential Equations (3.4) we choose the single-step Crank–Nicholson finite-difference scheme:

$$\frac{n_i^{j+1} - n_i^j}{\Delta t} = \frac{\Delta n_i}{\Delta t} = (1 - \alpha) f_i^j + \alpha f_i^{j+1}, \quad 0 \leq \alpha \leq 1, \quad i = 1\text{–}3. \tag{4.1}$$

For $\alpha \neq 0$ we have an implicit equations since f_i^{j+1} depends in rather complicated manner on the unknown populations n_i^{j+1}. For the temporal variable we write $t_{j+1} = t_j + \Delta t$ and all variables and functions in Equations (4.1) are also indexed by j and $j + 1$ at the corresponding times t_j and t_{j+1}, respectively. The scheme (4.1) is discussed for example by McClymont and Canfield (1982) and was also used by Klein, Stein, and Kalkofen (1976) for time-dependent Lyman continuum ionization in radiative shock dynamics computations. f_i^{j+1} in Equation (4.1) depend on the unknown populations n_l^{j+1} ($l = 1 - k$) and on the temperature-dependent functions $\Phi_i(T_e)$ and $\Omega_{ij}(T_e)$ at time t_{j+1}, which can easily be evaluated providing that we prescribe the temperature variations in the flaring plasma (Section 2). So the only nonlinear terms at the time t_{j+1} are various powers of n_l. To linearize the right-hand side of Equation (4.1), we simply write

$$n_l^{j+1} = n_l^j + \Delta n_l \quad l = 1 - k, \tag{4.2}$$

and in f_i^{j+1} we neglect all higher-order terms in Δn which arise due to multiplication of various n_l. For example,

$$(n_k^{j+1})^3 = (n_k^j + \Delta n_k)^3 \cong (n_k^j)^3 + 3(n_k^j)^2 \Delta n_k. \tag{4.3}$$

Equation (3.3) gives

$$\sum_{i=1}^{k} n_i^{j+1} = \sum_{i=1}^{k} n_i^j = n_{\mathrm{H}} = \text{const.}, \qquad \sum_{i=1}^{k} \Delta n_i = 0. \tag{4.4}$$

In this way we obtain a new system of *linear* algebraic equations for Δn_i ($i = 1 - k$) which has the general form

$$\mathbb{R}\Delta n = \mathbf{X}, \tag{4.5}$$

where the 4-dimensional matrix $\mathbb{R}$ and the vector $\mathbf{X}$ contain all the known functions of temperature and the level populations at the time t_j. Equations (4.5) are then solved by usual matrix inversion technique. However, in order to get a numerically stable method, we must use some kind of *adaptive time mesh*. In practice, at each time step we test the ratios $\Delta n_i/n_i^j$ for all $i = 1 - k$ and if the largest one is still higher as compared to a prescribed limit (say 10^{-2} or less), we divide the time step Δt by two and repeat the solution of Equations (4.5). Such a suitably selected limit justifies our neglect of higher-order terms in the linearization. Rather small time steps are needed when using Crank–Nicholson scheme, in order to minimize the dependence on α. An optimal time step for our models is $\Delta t \leq 10^{-2}$ s.

We have tested the stability of our code against the variations of α – no differences in the respective solutions have been found for two values $\alpha = 0.4$ and $\alpha = 0.8$, except of unimportant small oscillations for $\alpha = 0.4$, which do not affect the global behaviour of the solution (i.e., the smoothed curve is identical with that for $\alpha = 0.8$). The amplitude of such oscillations increases as α decreases and at small values of α a numerical instability can take place under certain conditions. All computations have been made with $\alpha = 0.8$.

An initial steady-state solution at $t = 0$ is obtained for each simulation (model) using the Equations (3.2) or (3.4) with $\partial n_i/\partial t = 0$. Note that in (3.4) we start with $C_{1j}^{nt} = 0$ at $t = 0$. These steady-state equations are linearized and solved iteratively by usual Newton–Raphson technique. As a test, we have computed the electron density and level populations for one selected atmospheric layer of VAL3C quiet-Sun model, the layer where Hα line center is formed. With $\rho_{32} = 0.02$ and $\rho_{k1} = 0$ (quiet-Sun conditions), we have arrived at a reasonable agreement with the exact computations of Vernazza, Avrett, and Loeser (1981) for their three-level hydrogen atom.

In order to check the consistency and accuracy of our time-dependent numerical solutions, we have rised the initial temperature $T_0 = 6500$ K to $T_m = 10^4$ K and allowed the level populations and the electron density to develop for sufficiently long time in order to reach a new stationary state at T_m. Independently, we have obtained this steady-state solution at T_m by solving the stationary equations using the Newton–Raphson iterations. Both the level populations as well as the electron density agreed quite well for these two solutions. Negligible differences were due to the fact that the stationary solution at T_m can be reached only at $t \to \infty$.

5. Hydrogen Excitation and Ionization

Using the approach described in previous sections, we have performed several numerical simulations to demonstrate temporal characteristics of the chromospheric hydrogen excitation and ionization which is due to a short-duration beam pulse or a series of such pulses. Let us start our discussion with three examples of a single-pulse heating

(Figures 1(a–c)), where $\Delta t_h = 0.1$ s (heating time equal to the beam duration), $\Delta t_c = 0.9$ s (cooling time necessary to reach the initial temperature), an initial temperature $T_0 = 6500$ K and the maximum temperature $T_m = 10^4$ K. In order to estimate the relative importance of non-thermal collisional excitation and ionization of hydrogen, we plot in each figure the solution for which these non-thermal rates have been 'switched-off'. Both the Hα source function $S(\mathrm{H}\alpha)$, as well as the electron density n_e are generally lower in this case, except for higher densities n_{H} and/or lower $\mathrm{d}F/\mathrm{d}t$, where non-thermal rates are of smaller importance. Computations have been made with ρ_{32} and ρ_{k1} equal to zero. There are two important features which we can immediately draw from Figures 1(a–c). First, it is clearly seen that for lower hydrogen densities, n_{H}, the relaxation times necessary to reach the initial state of plasma excitation and ionization are very long, of the order of tens of seconds at $n_{\mathrm{H}} = 10^{12}$–10^{14} cm^{-3}. This clearly indicates the necessity of using the time-dependent rate equations for such a non-stationary flare plasma and its modeling. For relatively short stationary-heating pulse (duration 5 s), a consistent solution of this kind was already obtained by FCM, but only for the case of a two-level hydrogen atom with continuum (i.e., not for Hα line – see the discussion below). The second important feature, which was not yet mentioned in the literature, is an abrupt *decrease* of $S(\mathrm{H}\alpha)$ at the beginning of the heating process –

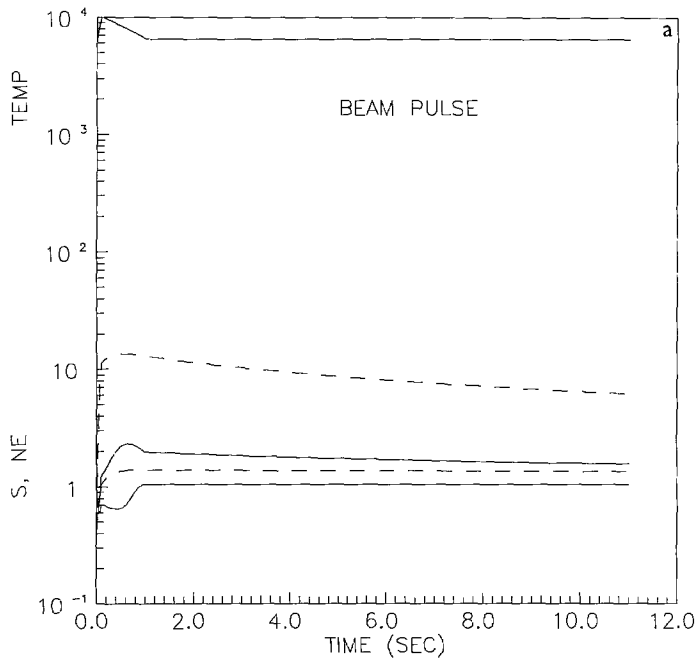

Fig. 1. Temporal variations of the kinetic temperature (TEMP), the electron density (NE – dashed lines), and an Hα soruce function (S – solid lines) for one beam pulse with $\Delta t_h = 0.1$ s, $\Delta t_c = 0.9$ s, $T_0 = 6500$ K, and $T_m = 10^4$ K. For NE and S, the lower curves correspond to the case when non-thermal collisional rates are ignored. Higher curves were obtained with $\mathrm{d}F/\mathrm{d}t = 10^4$ erg cm^{-3} s^{-1}. Both NE and S are normalized to their initial values at $t = 0$. (a) $n_{\mathrm{H}} = 10^{13}$ cm^{-3}, (b) $n_{\mathrm{H}} = 10^{14}$ cm^{-3}, (c) $n_{\mathrm{H}} = 10^{15}$ cm^{-3}.

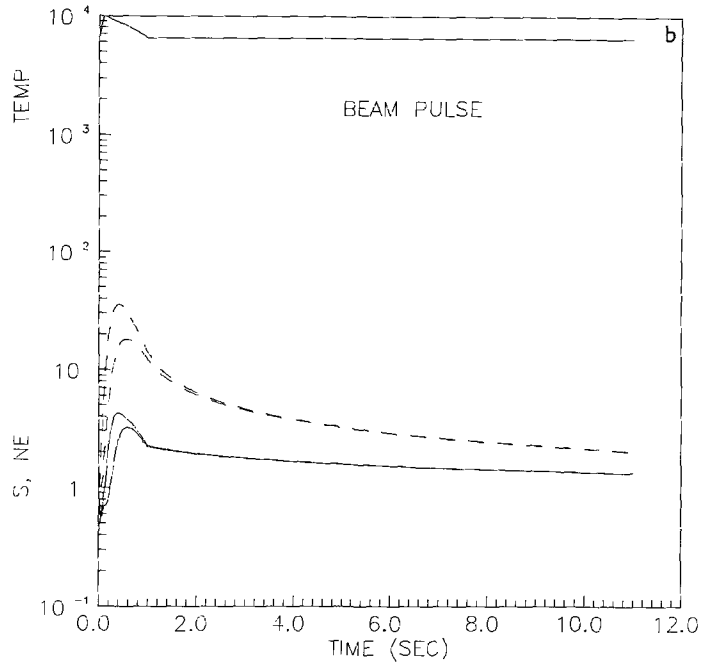
b
BEAM PULSE
TEMP
S, NE
10^4
10^3
10^2
10
1
10^{-1}
0.0
2.0
4.0
6.0
8.0
10.0
12.0
TIME (SEC)

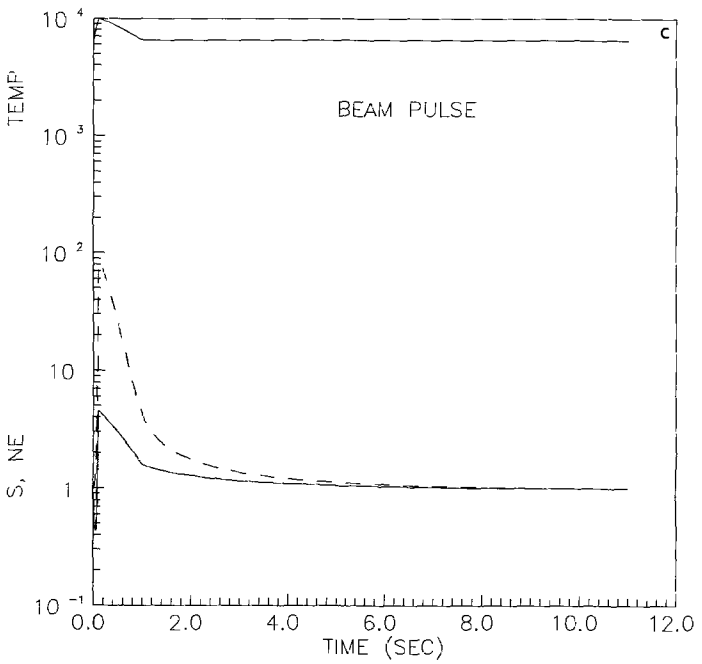
c
BEAM PULSE
TEMP
S, NE
10^4
10^3
10^2
10
1
10^{-1}
0.0
2.0
4.0
6.0
8.0
10.0
12.0
TIME (SEC)

Fig. 1 (cont.)

the rate of subsequent increase of $S(\mathrm{H}\alpha)$ then depends on the plasma density n_{H} and on the importance of non-thermal collisions (compare Figures 1(a–c)).

These newly discovered dips, which are present in all our simulations, deserve certain attention. It might seem at first sight that such an abrupt decrease of $S(\mathrm{H}\alpha)$ represents some kind of a numerical instability. Therefore, we have made several tests to avoid this uncertainty and found that the dips are practically insensitive to our choice of the parameter α in Equation (4.1) and to the time step Δt used. Moreover, we have tried three different shapes of the temperature profile on the interval Δt_h: a steep linear rise of $T(t)$, parabolic rise with zero derivative at $t = 0$, and the exponential increase of $T(t)$. All of them have led to almost identical shapes of dips. In Figure 2 we plot another example of a single pulse which is much broader with $\Delta t_h = \Delta t_c = 1$ s (a similar pulse was also studied by Karlický, 1990). In this figure we clearly see that the shape of dips (for both thermal and non-thermal processes) are rather shallow with no indications of any numerical instability. Note that the width of these dips and the time of their maximum depth depend on the plasma density and on the beam energy deposit, which is proportional to the incident energy flux of the beam. In order to see what happens with individual hydrogen level populations, we plot their temporal variations in Figures 3(a, b) for thermal and thermal + non-thermal collisions, respectively. These figures are qualitatively similar, indicating a steep rise of n_2 and n_3, while n_1 is gradually

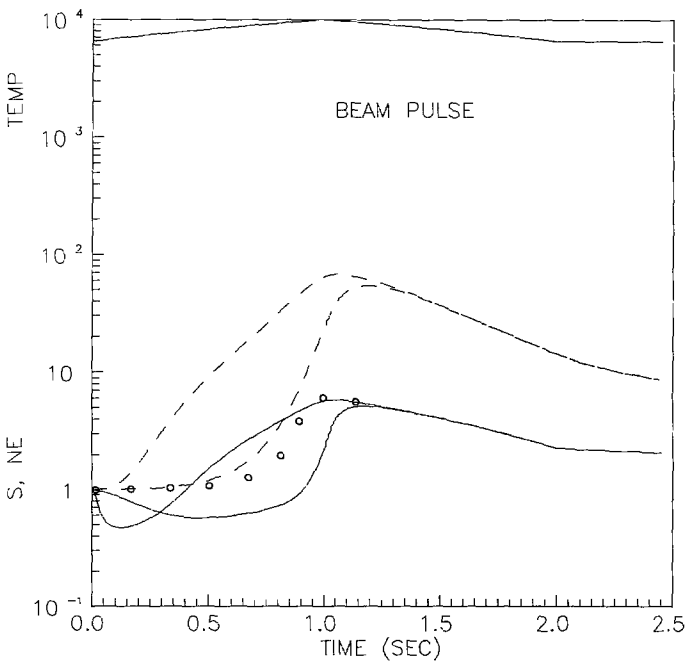

Fig. 2. Same as in Figure 1, but for a broader pulse with $\Delta t_h = \Delta t_c = 1$ s. Lower NE and a shallower dip in S correspond to the case when non-thermal collisional rates are ignored. Circles denote a test solution with $C_{13} = C_{12}$ and zero non-thermal rates (see the text). Higher curves were obtained with $\mathrm{d}F/\mathrm{d}z = 10^4$ erg cm^{-3} s^{-1}. n_{H} is equal to 10^{14} cm^{-3}.

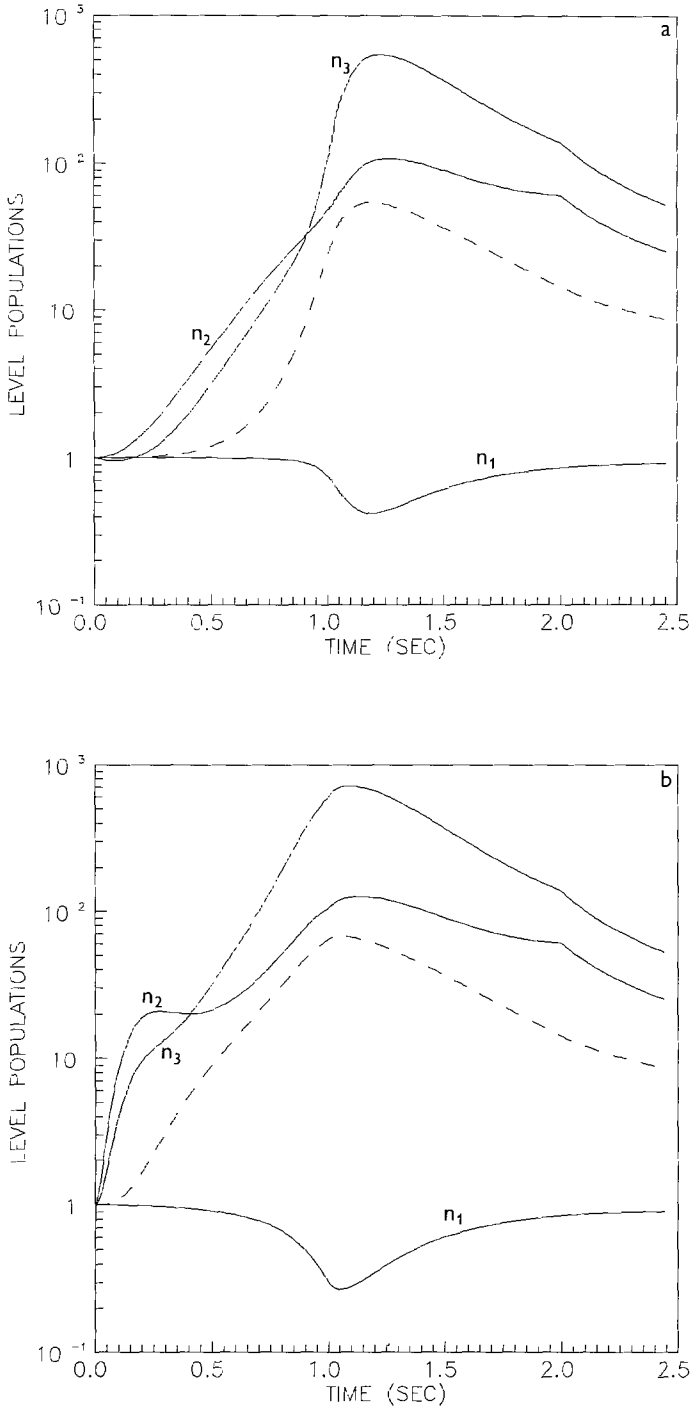

Fig. 3. Time-dependent hydrogen level populations (solid) and $n_e(t)$ (dashed) for the pulse model from Figure 2. All quantities are normalized to their initial values at $t = 0$. (a) Without non-thermal rates, (b) both thermal and non-thermal rates.

decreasing during the heating period. In the quiet-Sun chromosphere, n_2 and n_3 are determined by photo-recombinations in Balmer and Paschen continua, respectively, while under the flare conditions, both the second and third levels are populated collisionally from the ground state – see discussion in Canfield, Gunkler, and Ricchiazzi (1984). But since $\partial n_2/\partial t > \partial n_3/\partial t$ at the beginning of the pulse beam heating, $S(\mathrm{H}\alpha)$ decreases. We have found that this behaviour is a consequence of higher collisional rate $n_1(C_{12} + C_{12}^{nt})$ as compared to $n_1(C_{13} + C_{13}^{nt})$. Later on, when the electron density is also increased, the recombination processes seem to play again a role and the situation is qualitatively reversed, which leads to an increase of $S(\mathrm{H}\alpha)$. As a sensitivity test of the relative importance of C_{12} and C_{13}, we have set artificially $C_{13} = C_{12}$ and after recomputing the same models, we have found no dips in such a case (see circles in Figure 2). These dips are also absent at very high densities (starting roughly from $n_{\mathrm{H}} = 10^{18}\ \mathrm{cm}^{-3}$), which corresponds to the case of LTE. Indeed, in LTE we get

$$S(\mathrm{H}\alpha) \sim n_3/n_2 = (g_3/g_2)\, e^{-h\nu/kT} \tag{5.1}$$

and thus $S(\mathrm{H}\alpha)$ must follow the electron temperature variations.

For three identical pulses, the temporal behaviour of hydrogen ionization is displayed in Figures 4(a–c). Temperature variations for these three pulses are shown in Figure 5 above. This series of pulses represents a schematic model of real pulses as generated by Karlický (1990) and Heinzel and Karlický (1991). In contrast to a single pulse discussed above (with T linearly dependent on time), the temperature in these pulses

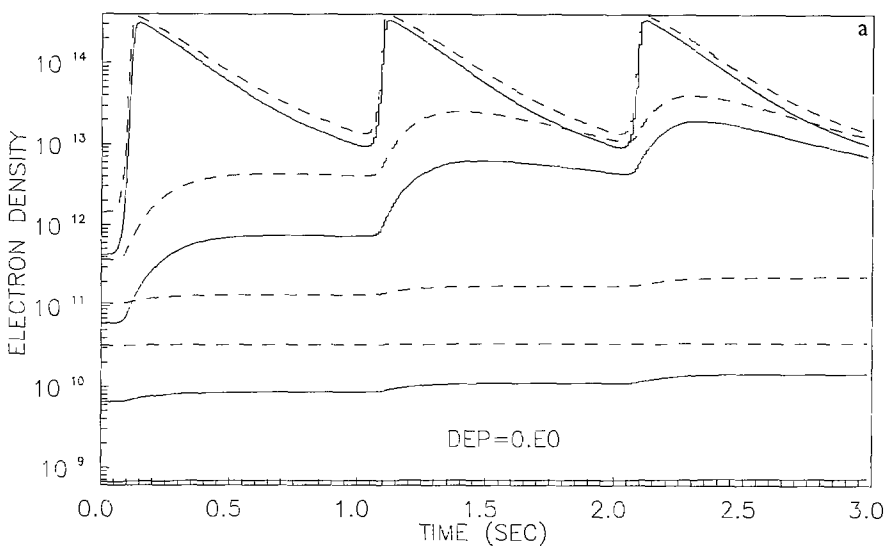

Fig. 4. Electron density n_e (cm^{-3}) versus time for multi-pulse beam heating models. Each of three subsequent pulses has $\Delta t_h = 0.1$ s and $\Delta t_c = 0.9$ s. $T_0 = 6000$ K, and $T_m = 10^4$ K (see Figure 5). Solid curves correspond to a layer where the Hα line center is formed, dashed ones are for deep layers where Hα wings originate. Higher curves correspond to higher values of $n_{\mathrm{H}} = 10^{12}$, 10^{13}, 10^{14}, and $10^{15}\ \mathrm{cm}^{-3}$, respectively. The parameter DEP denotes the value of $\mathrm{d}F/\mathrm{d}t$ ($\mathrm{erg\ cm}^{-3}\ \mathrm{s}^{-1}$). (a) DEP = 0.0, (b) DEP = 10^2, (c) DEP = 10^3.

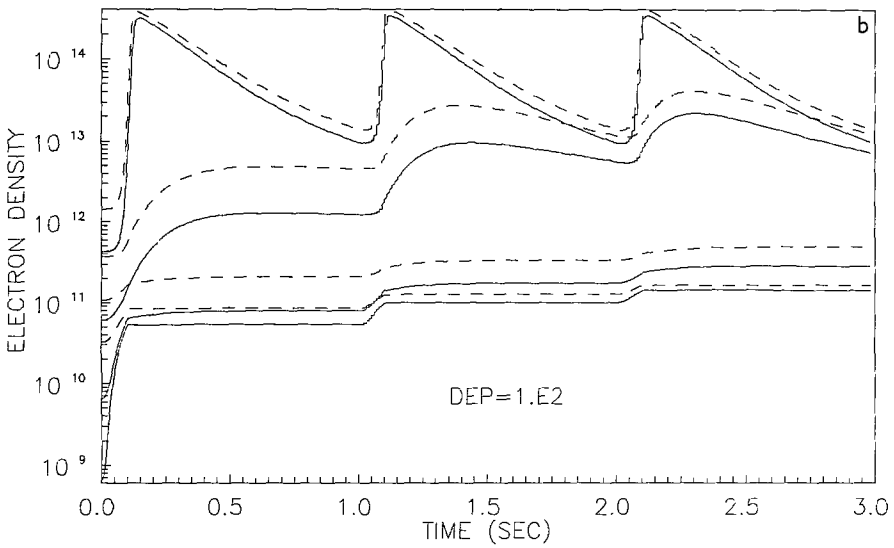

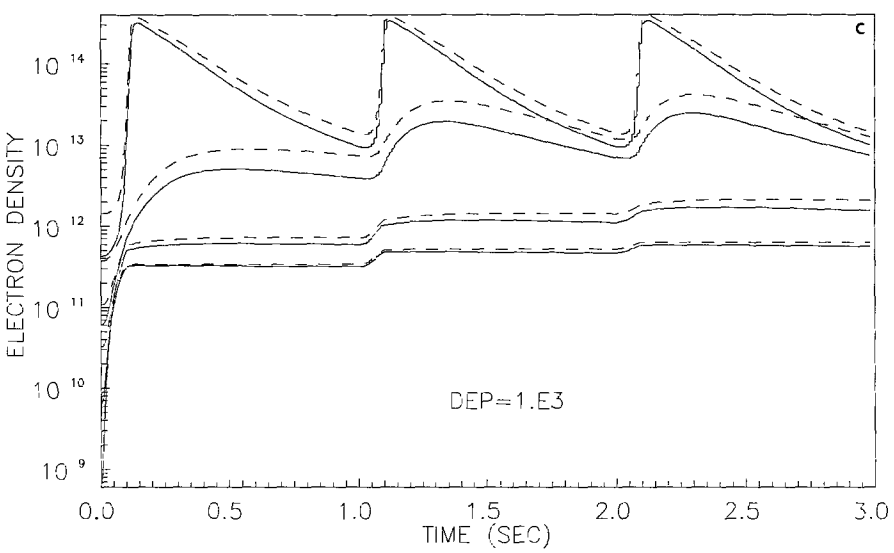

Fig. 4 (cont.)

rises and falls exponentially with time. However, as we have already mentioned, this difference has only marginal effect on our results. From Figures 4(b) ($dF/dz = 10^2$) and 4(c) ($dF/dz = 10^3$) we see how $n_e(t)$ varies with the hydrogen density n_H. As in the case of a single pulse, the relaxation to an initial state is rather long for $n_H < 10^{14}$ cm^{-3}. For $n_H = 10^{12}$ and 10^{13} cm^{-3}, the electron density is even continuously increasing with time and does not follow the temperature variations at all. At $n_H = 10^{14}$ cm^{-3}, the ionization peaks are somewhat lagged behind the temperature ones and n_e still gradually increases. Only at high densities, $n_e(t)$ follows more or less the temperature variations $T(t)$, although this electron density does not fall to its initial stationary value. In order to

demonstrate the relative importance of non-thermal collisional rates, we have computed the ionization of the plasma taking into account only thermal rates. The results are shown in Figure 4(a), which is to be compared with Figures 4(b) and 4(c). When non-thermal collisional rates are included, n_e is generally higher. However, whenever the electron density has reached sufficiently high value, the non-thermal rates become less effective and the curves for both DEP = 0 and DEP $\neq$ 0 differ only slightly. This takes place after a few pulses.

6. Temporal Variations of Hα Line Intensity

In order to obtain absolute Hα line intensities, we used a simple approximate formula valid for a constant-property flaring layer, irradiated from below by the photospheric radiation (Švestka, 1976)

$$I(\Delta\lambda) = r(\Delta\lambda)\, e^{-\tau(\Delta\lambda)} + (S/I_{\mathrm{cont}})\,[1 - e^{-\tau(\Delta\lambda)}]\,, \tag{6.1}$$

where $I(\Delta\lambda)$ is the emergent intensity at the disk-center, normalized to the continuum intensity $I_{\mathrm{cont}} = 4.077 \times 10^{-5}$ erg s^{-1} cm^{-2} sr^{-1} Hz^{-1}, $r(\Delta\lambda)$ is the residual Hα line intensity taken from David (1961), S represents the time-dependent source function and $\tau(\Delta\lambda)$ is the total optical thickness of the layer. All computations have been performed for $\Delta\lambda = 0$ Å (Hα line center) and for $\Delta\lambda = 1$ Å. We have assumed that the line center is formed under conditions with $\rho_{32} = 0.02$ and $\rho_{k1} = 0.5$ (see Section 3), while the wings at $\Delta\lambda = 1$ Å are formed much deeper in the flare atmosphere where both these radiative brackets tend to be zero. In the first case, a contribution to the line-center intensity from deeper layers is negligible, while for $\Delta\lambda = 1$ Å a less important contribution comes from surface layers. Therefore, in the formula (6.1) we insert two different depth-independent source functions, depending on $\Delta\lambda$. In a constant-property slab, the optical thickness is defined as

$$\tau(\Delta\lambda) = (\pi e^2/mc) f_{23} n_2 (\lambda_0^2/c) \varphi(\Delta\lambda) D\,, \tag{6.2}$$

where f_{23} is the oscillator strength, $n_2(t)$ is the second level population and D represents the geometrical thickness of the flaring layer (we take D = 100, 500, 1000, and 1500 km). $\varphi(\Delta\lambda)$ is the line absorption profile and we approximate it by the Voigt function, according to the Stark-broadening theory of Stehlé *et al.* (1983) who derived the Hα Stark width

$$\Delta\lambda_S[\text{Å}] = 1.073 \times 10^{-14} n_e (19.33 + \ln(2T^2/n_e))/T^{1/2}\,. \tag{6.3}$$

No microturbulent broadening was assumed.

In the following Figures 5–9, we present the results of our simulations for three identical pulses with $\Delta t_h = 0.1$ and $\Delta t_c = 0.9$ s (variations of the electron densities for these models have been discussed in the preceding Section 5). In all these figures we again observe short-duration dips at both wavelengths. Their depths and widths are sensitive to n_{H} and to the importance of non-thermal collisional rates which are proportional to $\mathrm{d}F/\mathrm{d}z$ (denoted as DEP in these figures). Although temporal variations

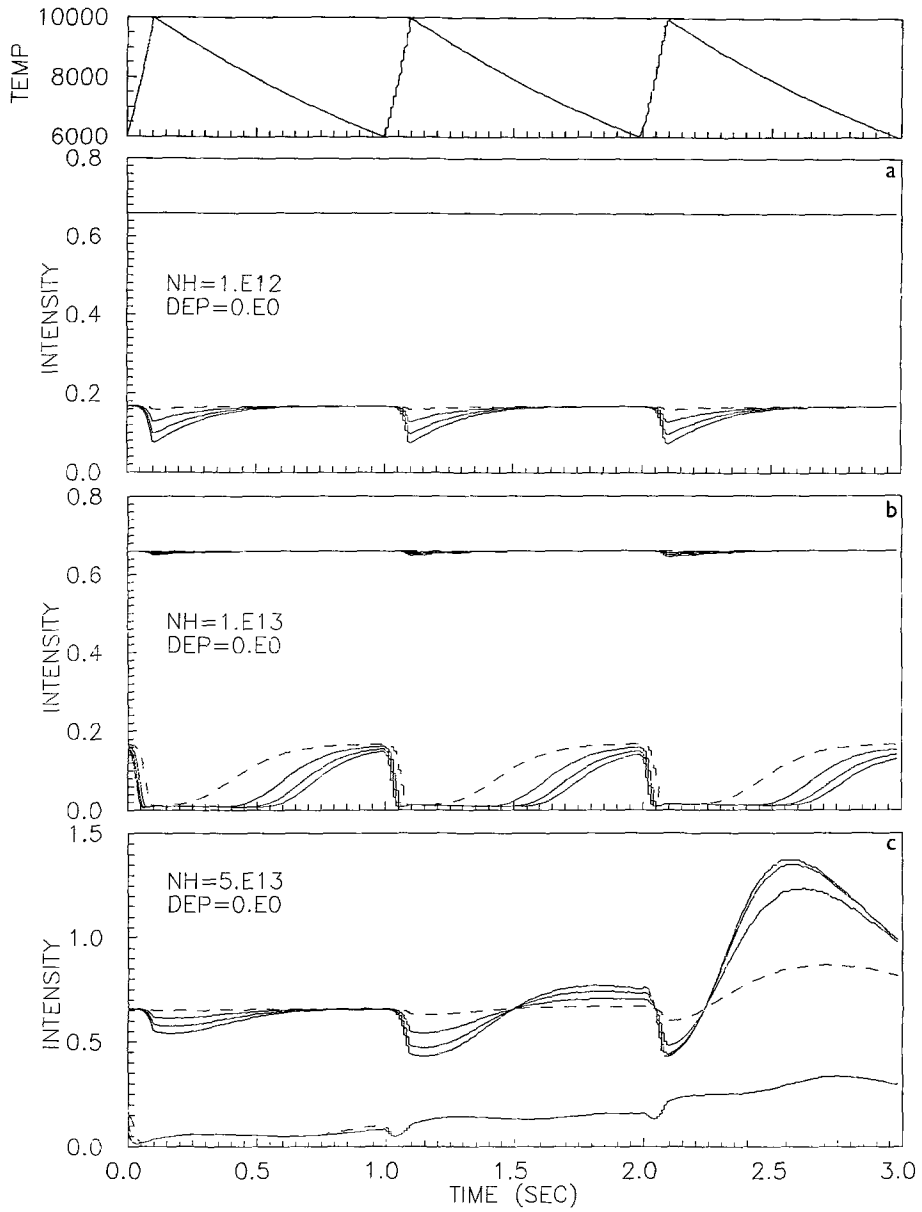

Fig. 5. Temporal variations of the Hα line intensity for multi-pulse beam heating models (for $n_e(t)$ see Figure 4). The line intensities are normalized to the continuum. The curves in a lower part of each figure correspond to $\Delta\lambda = 0$ Å, those in an upper part belong to $\Delta\lambda = 1$ Å. For both these wavelengths we display four curves corresponding to $D = 100$ km (dashed line), $D = 500$, 1000, and 1500 km (subsequent solid lines). All figures are labeled by n_H (cm^{-3}) and by dF/dt (erg cm^{-3} s^{-1}) – DEP. The upper panel shows the corresponding temperature pulses $T(t)$.

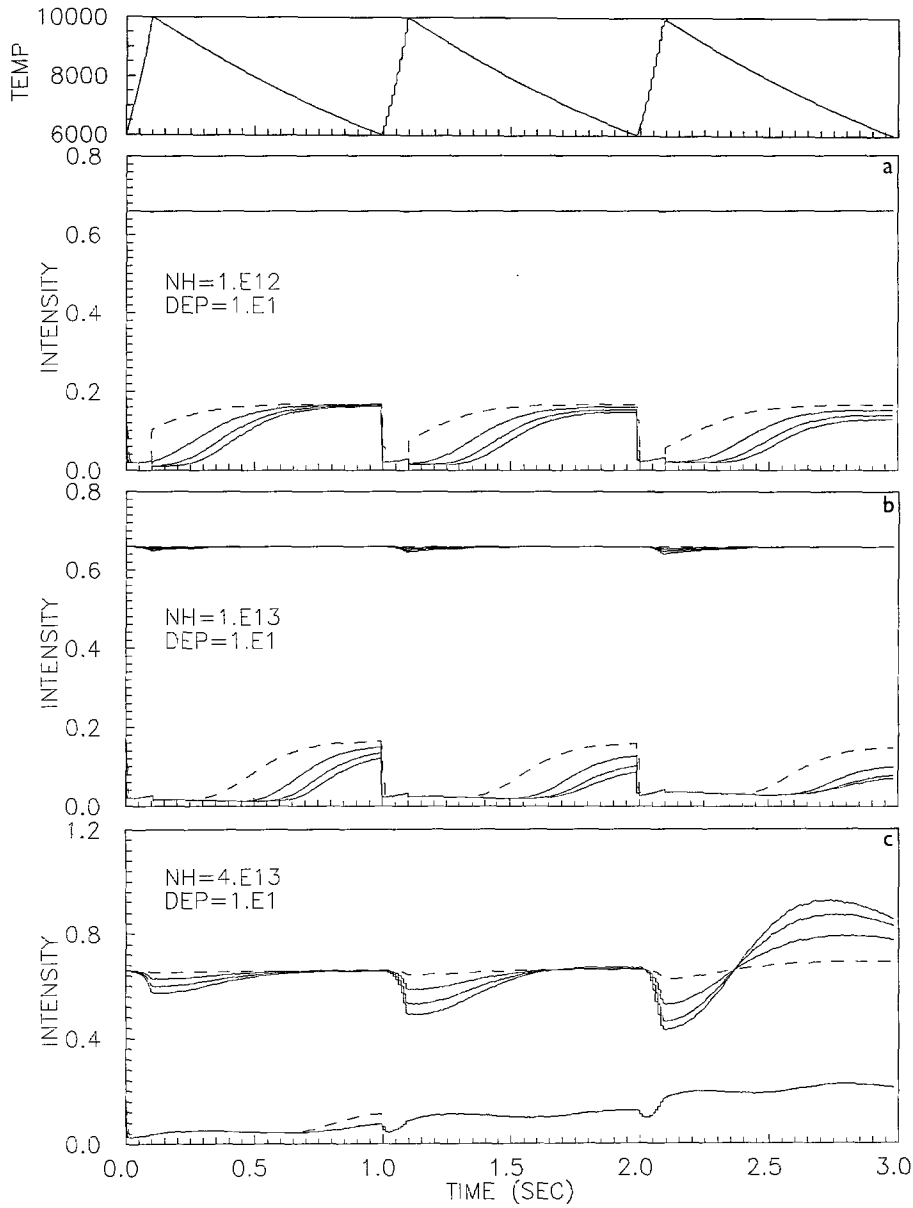

Fig. 6. Same as in Figure 5, but for the model parameters indicated.

of the Hα emission depend rather sensitively on the structure of temperature pulses $T(t)$, we use for this exploratory study only the range between $T_0 = 6000$ K and $T_m = 10^4$ K. Hydrogen densities, on the other hand, take all reasonable values which can be met under chromospheric flare conditions. Maximum energy deposit dF/dz in Karlický's (1990) models is of the order of 10^2 erg cm^{-3} s^{-1}. We include the case with DEP = 0

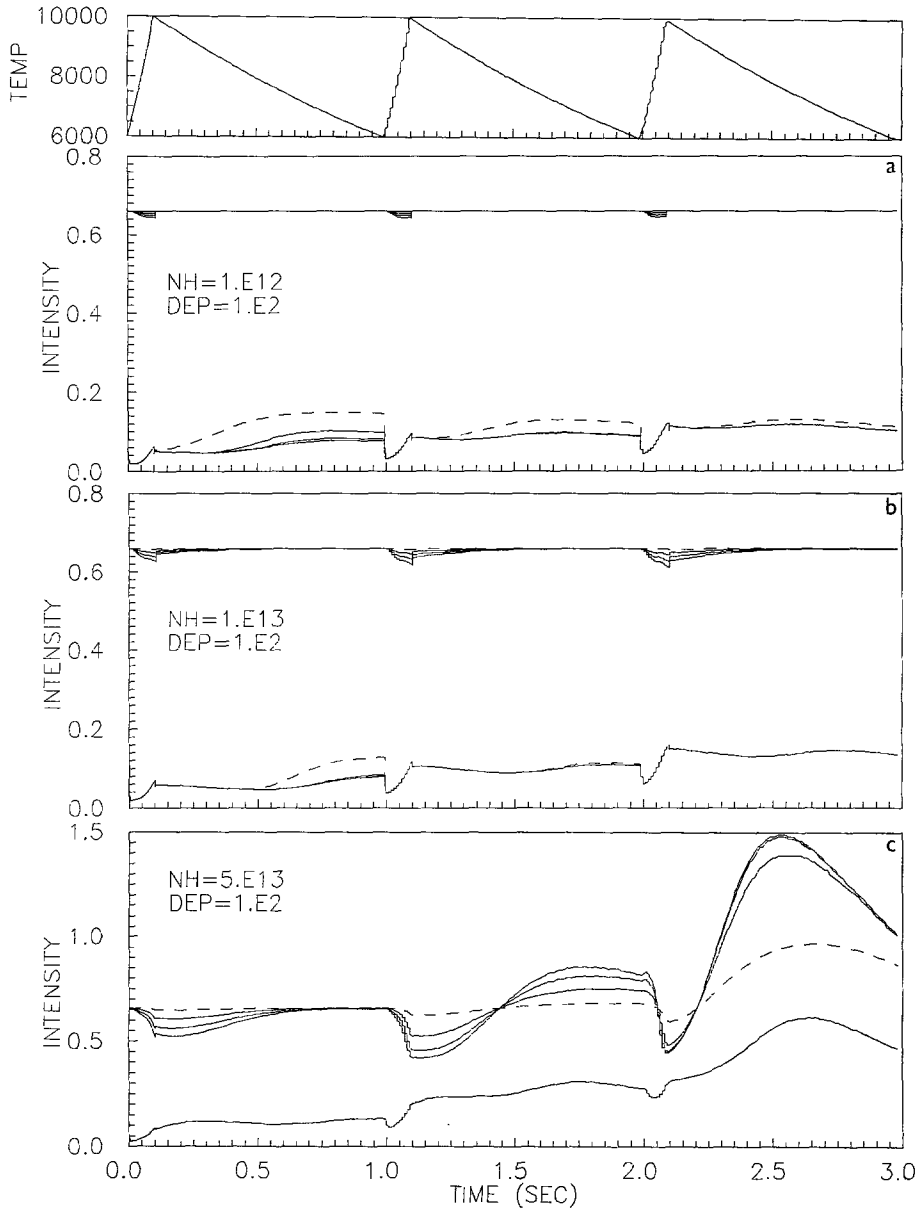

Fig. 7. Same as in Figure 5, but for the model parameters indicated.

just to demonstrate the effect of non-thermal collisional rates on the resulting Hα profiles. In these figures, the Hα line-center intensity is approximately equal to 0.15 at t = 0 s (i.e., the quiet-Sun value, see Figure 5) and then it rapidly decreases whenever the pulse is switched-on. This is not well resolved in some figures, especially for higher values of n_H and DEP. Note also the different intensity scales in various parts of these figures.

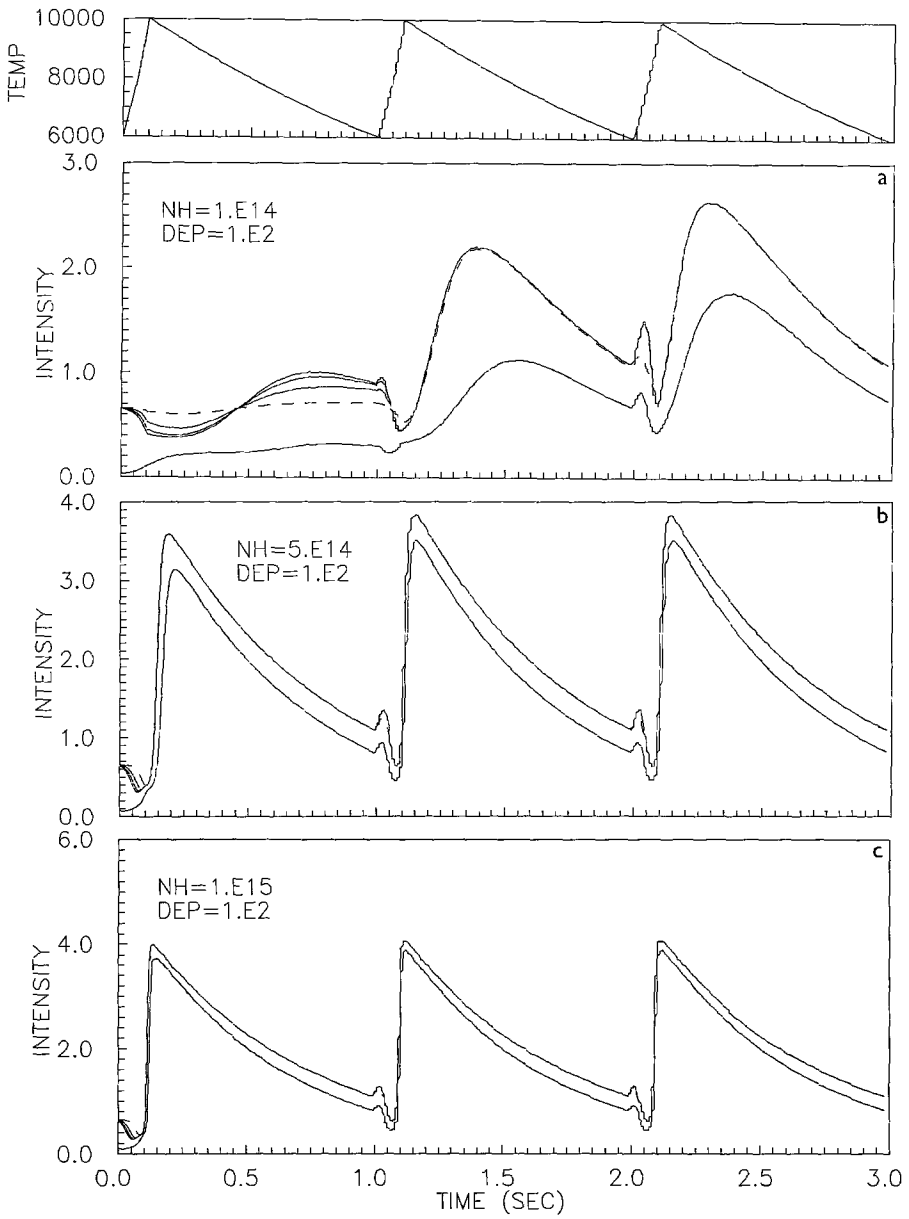

Fig. 8. Same as in Figure 5, but for the model parameters indicated.

The most interesting feature is the presence of dips, both in the line core as well as in the wings of Hα. Under certain conditions, these dips can be rather broad, comparable to the duration of one temperature pulse (see Figure 6). There are two time scales of Hα intensity variations. First, the dips or peaks vary on the scales Δt_h or Δt_c, and second, a gradual increase of Hα can be observed during several pulses, e.g.,

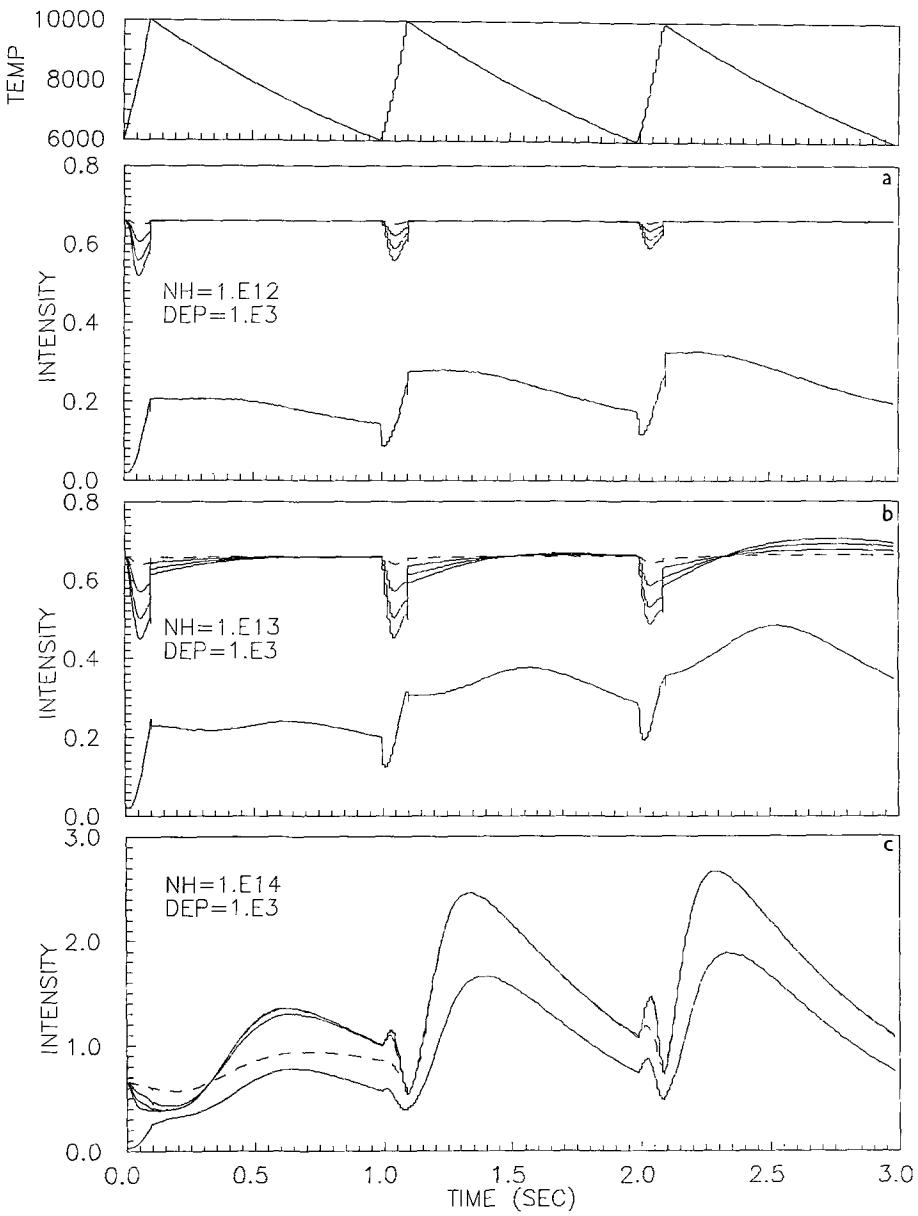

Fig. 9. Same as in Figure 5, but for the model parameters indicated.

Figures 7(c), 8(a), or 9. Therefore, a series of very short beam pulses can be generally responsible for a gradual rise of Hα emission, while on the time scales less than one second various fine-structure features can be detected indicating the short-duration beam heating.

Finally, in the last Figure 10 we try to compare our simulations with those of Canfield

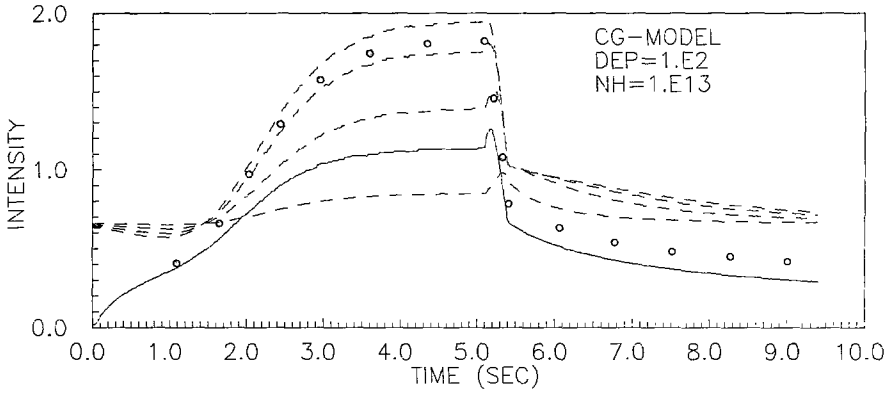

Fig. 10. The beam heating model similar to that of Canfield and Gayley (1987). $\Delta t_h = 0.1$ s, then a stationary heating lasts for 5 s, and finally $\Delta t_c = 0.3$ s. $T_0 = 6000$ K, $T_m = 10^4$ K. For such a box-like temperature pulse we display Hα intensities at $\Delta\lambda = 0$ Å (solid line) and at $\Delta\lambda = 1$ Å (dashed lines corresponding to $D = 100$ km (lowest one), $D = 500$, 1000, and 1500 km). $n_H = 10^{13}$ cm^{-3}, DEP $= 10^2$. Circles represent a line-center solution, but with $\rho_{k1} \equiv 0$.

and Gayley (1987). For the beam energy deposit rate comparable to that of these authors and for an intermediate density $n_H = 10^{13}$ cm^{-3}, we plot the temporal behaviour of Hα intensity at the line-center and at $\Delta\lambda = 1$ Å. This can be compared with Figure 2 of Canfield and Gayley (1987). Since we deal with a static atmosphere and do not solve the transfer problem explicitely, any detailed quantitative comparison is not possible. However, the general qualitative behaviour of $I(t)$ is similar, except at the very beginning of the pulse, where we have again obtained typical dips which are a consequence of higher population rate of the second level as compared to the third one. Although Canfield and Gayley (1987) use a four-level hydrogen atom with continuum, they start with $n_e(t)$ taken from previous two-level plus continuum simulations of FCM. Moreover, to solve the transfer problem at a given time, these authors set $\partial n_2/\partial t = \partial n_3/\partial t = \partial n_4/\partial t = 0$ in the rate equations, which seems to be a reasonable approximation, providing that $n_e(t)$ is already known. However, all these differences from our approach, which is consistent from the viewpoint of the solution of time-dependent rate equations for a three-level plus continuum model atom, may lead to the absence of dips in Figure 2 of Canfield and Gayley (1987). Another reason could be the width Δt_h which we take here to be 0.1 s. For even smaller Δt_h, the dips are very narrow and may not be numerically resolved.

7. Conclusions

In this paper we have presented the first numerical simulations of temporal variations of hydrogen plasma excitation and ionization on time intervals of less than one second. These short-duration variations are due to fast spiky changes of the kinetic temperature and non-thermal collisional rates. Such temperature spikes represent a chromospheric response to a series of short-duration electron beam pulses which are assumed to heat

the flare plasma. A consistent numerical solution of time-dependent rate equations for a three-level hydrogen atom with continuum allowed us to predict theoretically a qualitative behaviour of the Hα line intensity variations on very short time scales. Our Hα line temporal profiles, evaluated at the line center and for $\Delta\lambda = 1$ Å, can be qualitatively compared with some recent observations obtained with high temporal resolution.

During several beam pulses, Hα intensity gradually increases on longer time scales of several seconds. With the resolution comparable to a temperature pulse duration (one second in our case), the Hα emission peaks seem – under favourable conditions – to correlate with the temperature pulses and thus also with HXR emission. However, these intensity maxima typically lag behind the temperature peaks, which is a consequence of the fine structure Hα intensity dips formed at the beginning of each pulse. This effect is most pronounced at lower n_{H}. Since these fine structure features are rather sensitive to the plasma density and various beam characteristics, they represent a potential diagnostics tool for studying the electron beam heating. It is worth noting that these sub-second variations exhibit a different behaviour in the line core and in the wings of Hα, which further supports their diagnostical importance.

Concerning the electron densities, we have arrived at an increase of n_e by 1–2 orders of magnitude during the pulse beam interaction with the ambient plasma. This is comparable to typically observed values. Again, both short-term (spiky) as well as gradual variations of n_e can be observed. Ionization changes do follow the structure of temperature pulses at rather high plasma densities ($n_{\mathrm{H}} \cong 10^{15}$ cm^{-3}), while for lower n_{H} the ionization peaks (i.e., the maxima of $n_e(t)$) are lagged behind the maxima of $T(t)$. At low densities of the order of 10^{12}–10^{13} cm^{-3}, $n_e(t)$ is continuously increasing and does not follow the temperature variations at all. This is the consequence of a relatively long relaxation time for hydrogen recombination.

Acknowledgements

The author is indebted to Drs M. Karlický and J.-C. Hénoux for numerous stimulating discussions and for providing him with their new flare models.

References

Aboudarham, J. and Hénoux, J.-C.: 1986, *Astron. Astrophys.* **168**, 301.
Auer, L., Heasley, J., and Milkey, R.: 1972, *Kitt Peak Natl. Obs. Contr.* No. 555, Kitt Peak National Obs., Tucson.
Avrett, E. H.: 1988, private communication.
Brown, J. C.: 1973, *Solar Phys.* **31**, 143.
Canfield, R. C. and Gayley, K. G.: 1987, *Astrophys. J.* **322**, 999.
Canfield, R. C. and Puetter, R. C.: 1981, *Astrophys. J.* **243**, 381.
Canfield, R. C. and Ricchiazzi, P. J.: 1980, *Astrophys. J.* **239**, 1036.
Canfield, R. C., Gunkler, T. A., and Ricchiazzi, P. J.: 1984, *Astrophys. J.* **282**, 296.
David, K. H.: 1961, *Z. Astrophys.* **53**, 37.
Dumont, S. and Collin-Souffrin, S.: 1985, *Astron. Astrophys.* **144**, 245.
Emslie, A. G.: 1978, *Astrophys. J.* **224**, 241.
Feautrier, N. and Sahal-Bréchot, S.: 1991, private communication.

Fisher, G. M., Canfield, R. C., and McClymont, A. N.: 1985a, *Astrophys. J.* **289**, 414 (FCM).
Fisher, G. M., Canfield, R. C., and McClymont, A. N.: 1985b, *Astrophys. J.* **289**, 425 (FCM).
Fisher, G. M., Canfield, R. C., and McClymont, A. N.: 1985c, *Astrophys. J.* **289**, 434 (FCM).
Graeter, M.: 1990, *Solar Phys.* **130**, 337.
Heinzel, P. and Karlický, M.: 1991, in preparation.
Heinzel, P., Gouttebroze, P., and Vial, J.-C.: 1987, *Astron. Astrophys.* **183**, 351.
Hummer, D. G.: 1982, *J. Quant. Spectr. Rad. Trans.* **27**, 569.
Ivanov, V. V.: 1973, *Transfer of Radiation in Spectral Lines*, NBS SP-285, US Dept. Commerce, Washington, D.C.
Karlický, M.: 1990, *Solar Phys.* **130**, 347.
Karlický, M. and Hénoux, J.-C.: 1991, *Bull. Astron. Inst. Czech.* **42**, 22.
Kiplinger, A. L., Dennis, B. R., Orwig, L. E., and Chen, P. C.: 1988, *Proc. First Max'91 Workshop*, Kansas City, p. 214.
Kitahara, T. and Kurokawa, H.: 1990, *Solar Phys.* **125**, 321.
Klein, R. I., Stein, R. F., and Kalkofen, W.: 1976, *Astrophys. J.* **205**, 499.
Kundu, M. R., Woodgate, B., and Schmahl, E. J. (eds.): 1989, *Energetic Phenomena on the Sun*, Kluwer Academic Publishers, Dordrecht, Holland.
Kurokawa, H.: 1986, in D. Neidig (ed.), *The Lower Atmosphere of Solar Flares*, Proc. NSO/SMM Flare Symp., Sunspot, p. 51.
Mariska, J. T., Emslie, A. G., and Li, P.: 1989, *Astrophys. J.* **341**, 1067.
McClymont, A. N. and Canfield, R. C.: 1983, *Astrophys. J.* **265**, 483.
Mihalas, D.: 1978, *Stellar Atmospheres*, 2nd ed., W. H. Freeman, San Francisco.
Ricchiazzi, P. J. and Canfield, R. C.: 1983, *Astrophys. J.* **272**, 739.
Rybicki, G. B.: 1984, in W. Kalkofen (ed.), *Methods in Radiative Transfer*, Cambridge University Press, Cambridge, p. 21.
Stehlé, C., Mazure, A., Nollez, G., and Feautrier, N.: 1983, *Astron. Astrophys.* **127**, 263.
Švestka, Z.: 1976, *Solar Flares*, D. Reidel Publ. Co., Dordrecht, Holland.
Vernazza, J. E., Avrett, E. H., and Loeser, R.: 1981, *Astrophys. J. Suppl.* **45**, 635.